Hierarchical Structure of Porous Silicon Nitride Ceramics with Aligned Pore Channels Prepared by Ice-Templating and Nitridation of Silicon Powder

Dong Seok Kim and Do Kyung Kim*

Department of Materials Science and Engineering, Korea Advanced Institute of Science and Technology (KAIST), 291 Daehak-ro, Yuseong-gu, Daejeon 305-701, Korea

A unique hierarchical porous structure of silicon nitride ceramic with 76.5% porosity is fabricated by combining an ice-templating method and nitridation for a silicon powder. The porous silicon nitride ceramics were composed of a lamellar structure with aligned pore channels and ceramic walls filled with fibrous whiskers. This study is focused on the influences of freezing rate on the microstructures and properties of the silicon nitride ceramics. The properties were characterized by compressive strength and gas permeability, which were shown to vary with controlled microstructure. The compressive strength and the permeability reached up to 32.2 MPa and 0.035^{-12} m^2, respectively.

Introduction

Porous ceramics have been widely used for industrial applications such as filters, gas distributors, catalyst supports, high-temperature thermal insulation, implantable bio-ceramics, and so on.[1] Due to their structures and the nature of ceramics, porous ceramics exhibit a unique combination of properties, including low thermal conductivity, low thermal mass, low dielectric constant, low density, high thermal shock resistance, high wear resistance, high specific strength, and high permeabilities for gases and liquids, making them indispensable in a wide range of engineering applications. These characteristics and properties of porous ceramics are determined by their pore geometries, including pore size, shape, distribution, and connectivity. Therefore, it is important to control pore structures to have suitable properties for particular applications.

The ice-templating method (i.e., freeze-casting) is a fabrication method used to produce porous ceramics. The method has recently attracted attention as a novel technology for the fabrication of porous bulk ceramics with unique hierarchical pore structures.[2–4] The method consists of simple steps, beginning with preparing a ceramic powder slurry with specific concentrations for a particular porosity. The slurry is then frozen under controlled cooling conditions. After freezing, the sample is freeze-dried under low pressure, causing ice crystals in the sample to sublimate, producing porosity in the sample by direct replication of the ice crystal structure. If the slurry is cooled and frozen in certain direction of the temperature gradient, ice crystals grow continuously along the freezing direction throughout the sample slurry, typically providing lamellar pore channels in the product material.[5,6] The pore structure can be modified by the growth shape of these ice crystals, which are affected by the freezing conditions used, including the freezing methods employed,[7,8] freezing rates,[9–11] additives,[12,13] and using other freezing vehicles instead of water.[14,15] Finally, the porous structure can be sintered to consolidate the ceramic particles, producing rigid porous bulk ceramic materials. The method of ice-templating for porous ceramics has been studied for application in various fields such as bio-ceramics,[16,17] energy applications,[18,19] dielectric applications,[20] and scaffold for composites[21,22] with various ceramic materials.

One of the engineering ceramic materials, silicon nitride (Si_3N_4) is a good candidate for various applications at high temperatures due to its high elastic modulus, low thermal expansion, and good stability at high temperatures.[23,24] Particularly, silicon nitride ceramics with a designated porosity can be used in filter applications and other engineering fields due to high specific strength and high permeability to gases and liquids.[25,26] Fabricating silicon nitrides using a reaction bonding process is one of the methods to produce bulk silicon nitrides. A silicon powder compact reacts with nitrogen at elevated temperatures to form reaction-bonded silicon nitrides; this process has the advantage of achieving near-net shaping and lowering the sintering temperature compared to the direct sintering of silicon nitride powder.

In this study, to achieve high strength and highly permeable porous silicon nitride ceramics, we attempted

*dkkim@kaist.ac.kr

to fabricate porous silicon nitride ceramics using the ice-templating method followed by nitridation with silicon powder; a unique hierarchical porous silicon nitride ceramic was presented. The microstructures of the as-templated silicon structure and the porous silicon nitride structures after the nitridation were observed to investigate the formation mechanism of the porous silicon nitride ceramics and the influences of freezing rates on the microstructures. Compressive tests and gas flow tests were performed to determine the structural integrity and gas permeability of the materials as well. This study would provide some information and inspirations to readers that have interests in not only the reaction bonding silicon nitride and the freeze-casting method, but also porous materials, and filter materials.

Experimental Procedure

To fabricate hierarchical porous silicon nitride structures, porous silicon structures were prepared first and then subjected to a nitridation process. The porous silicon structures were fabricated by the ice-templating method with water-based silicon slurries. The silicon slurries were prepared by mixing distilled water with 20 vol % of silicon powder (purity ≥ 98.9 wt%; d_{50}=7 μm; Sicomill grade 4, metal basis 99%, Permascand AB, Ljungaverk, Sweden), Polyvinyl Alcohol (PVA; Sigma Aldrich, St. Louis, MO) as a binder and Polyvinyl Pyrrolidone (Sigma Aldrich) as a dispersant; the binder and the dispersant were both added at 2 wt % of the silicon powder. 1 wt.% of glycerol (Sigma Aldrich) compared to silicon powder was also added as an anti-freezing agent. The anti-freezing agent was needed to reduce the freezing rate not to reach to the critical velocity that silicon particles will be entrapped randomly by the freezing front, resulting in loss of the lamellar structure.[27] Silicon powder and additives were mixed, preceded by dissolving the PVA completely by heating the distilled water to 80°C. The mixture of the contents was stirred with a magnetic bar for 30 min and de-aired in a vacuum desiccator for 5 min.

The prepared slurries were frozen unidirectionally from bottom to top in a cylindrical mold which was made of polydimethylsiloxane (Sylgard 184; Dow Corning, Midland, MI) with an inner diameter of 20 mm. The mold was placed on the top of a copper rod of which the bottom side of the rod was dipped in liquid nitrogen to initiate cooling. The cooling rates were controlled with a thermocouple and a ring heater covering around the copper rod. The freezing rate of the sample (i.e., the ice-front velocity) was maintained to be nearly steady by controlling the cooling rate.[10,28] The average freezing rate of the slurries was mea-sured by dividing the height of a frozen sample by the time until the sample was frozen completely. The silicon slurry was frozen with four different freezing rates, 5, 10, 25, and 60 μm/s. After freezing, the frozen samples were demolded and loaded into a commercial freeze dryer (FreeZone 2.5; Labconco, Kansas City, MO). The samples were maintained in a vacuum of 0.035 mbar for 24 h.

The freeze-dried samples were placed on a graphite plate that was coated with boron nitride and then heated in 5% H_2/95% N_2 atmosphere flowing at 80 cc/min in a horizontal alumina tube furnace. A stepwise heating cycle was used for the nitridation: (i) rapid heating to 1200°C (300°C/h), (ii) heating 1200–1300°C for 1.5 h (15.6°C/h) followed by a 1-h hold at the same temperature, the flowing gas was changed 5% H_2/95% N_2 to 100% N_2 at the point to the end, (iii) heating to 1350°C for 3.5 h (14.4°C/h) followed by a hold at 1350°C for 2.5 h, (iv) heating to 1450°C for 5.5 h (18°C/h) and holding at 1450°C for 2.5 h, and (v) finally, the temperature decreased to RT with the rate of 300°C/h.

The morphology of the porous silicon structure and the silicon nitride structure was determined by scanning electron microscopy (FE-SEM; XL30, FEG; Philips, Eindhoven, the Netherlands) and binocular optical stereomicroscopy (BH2-UMA, Olympus, Tokyo, Japan). The distribution of pore size was characterized using mercury porosimetry (Autopore IV 9510l; Micromeritics, Norcross, GA). Weight change due to nitridation was obtained and used for estimating the nitridation ratio; and phase analysis was conducted by X-ray diffraction analysis (XRD; Rigaku, D/Max-2500, Tokyo, Japan).

Compressive strength tests were performed to evaluate the structural integrity of the samples. The samples were cut to be $5 \times 5 \times 5 \pm 0.1$ mm^3 and loaded along the freezing direction at a crosshead speed of 6 mm/min using a screw-driven load frame (Unitech; R&B, Daejeon, Korea).

The flow rates of nitrogen gas through the sample were measured using disk specimens with thickness $t \leq 1$ mm from the porous structure except the part of 1–2 mm for both bottom and top of the samples. The flow rate was recorded as the input pressure was gradually increased using a porometer (CFP-1200-AEL; Porous Materials, Ithaca, NY) to obtain the Darcian permeability.

Result and Discussion

Figure 1 shows the SEM images of an ice-templated porous silicon structure frozen at a rate of 25 μm/s. Figure 1a–d presents the lateral cross section of the green body sample perpendicular to the freezing direction. The
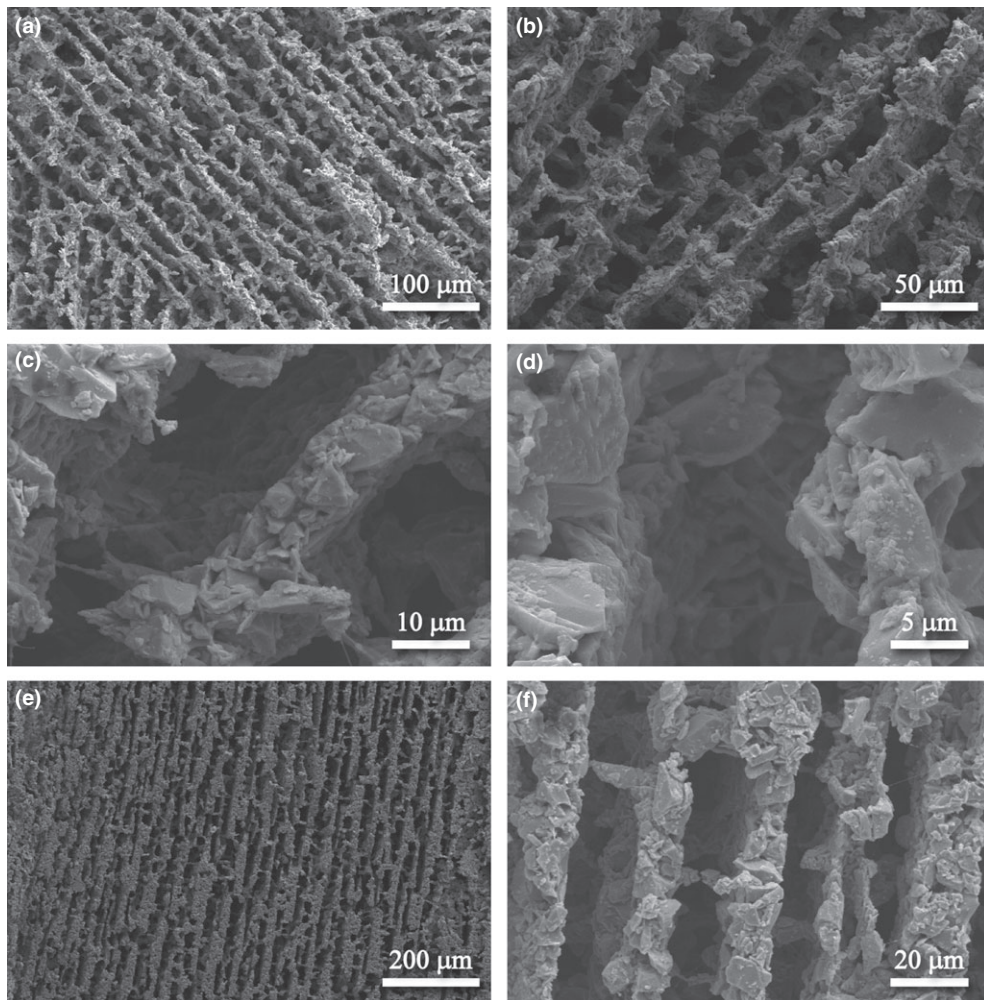
Fig. 1.   SEM images of a cross-sectional view of an ice-templated porous silicon structure (a–d) perpendicular to the freezing direction and (e–f) parallel to the freezing direction. The porous structure is formed with lamellar planes; some bridges also formed with silicon particles.

porous structure is shown to be a lamellar architecture like many other studies using the typical unidirectional ice-templating method as mentioned in the introduction. Macroscopically aligned pore channels formed over the entire sample. The lamellar walls of the silicon particles were aligned in a certain domain of random orientations. Some dendritic protrusions of silicon particles are present on the surface on the lamellar walls and even extended into adjacent lamellar walls, forming connections like bridges. These ceramic bridges were thought have arisen from local ice crystal tip splitting and engulfment of particle agglomerates created by particles repelled from the ice–water interface and subsequent tip healing.[4] Figure 1c,d shows microscopic details of the lamellar wall configuration and interconnection of silicon particles in higher magnification. A few layers of silicon particles were found to be glued together with the binder to form a densely packed lamellar wall structure and that was due to rejection and redistribution of the silicon powder by the ice-crystal growth in the freezing step. Figure 1e,f shows the cross section of the sample parallel to the freezing direction. The lamellar walls and the pore channels were straight along the freezing direction throughout the porous green bodies.

After the nitridation, the ice-templated green body samples were turned into light gray color. The bulk density of the nitrided samples was determined by the Archimedes' method and weight to volume ratio, the result was not much varied in two methods. The density was approximately 0.75 ± 0.08 g/cm³, which indicates that the structure has 76.5% of porosity.

The nitridation rate (R_N) of the samples prepared in this study was measured by weight change and using following Eq. (1):

$$R_{\mathrm{N}}(\%) = \frac{W_{\mathrm{f}} - W_{\mathrm{i}}}{W_{\mathrm{si}}} \times \frac{100}{66.5} \times 100, \qquad (1)$$

where W_{f} is the weight of the nitride compacts composed of the reaction products Si_3N_4, unreacted Si, and additives; W_{i} is the weight of the green bodies of the silicon compact; and W_{si} is the weight of the amount of silicon in the initial green body. The equation implies that 66.5% of the weight is gained via the nitridation of Si to Si_3N_4, assuming both perfect nitridation and zero weight loss of the compact mixtures during the nitridation process.[29] The results were averaged to be $92.4 \pm 0.5\%$. The high rate of nitridation is also shown in the X-ray diffraction patterns. Figure 2 represents X-ray diffraction patterns of the porous silicon nitride structure at a freezing rate of 25 μm/s. Si peaks were not detected on the diffraction patterns shown in Fig. 2; thus nitridation was considered to be nearly complete. The diffraction peaks were related to the α (JCPDS: 09-0250) and β (JCPDS: 33-1160) phases of Si_3N_4. The relative β/α phase fraction was estimated using the relation between the intensities of the (210) diffractions of both phases, according to Gazzara and Messier:[30]

$$\varphi_\beta = \frac{I_\beta^{(210)}}{I_\beta^{(210)} + I_\alpha^{(210)}}. \qquad (2)$$

The fractional ratio of β/α was calculated to be 7.6%, which indicates that the porous structure was composed primarily of α-Si_3N_4. It was determined that the dominance of α-Si_3N_4 was affected by the presence
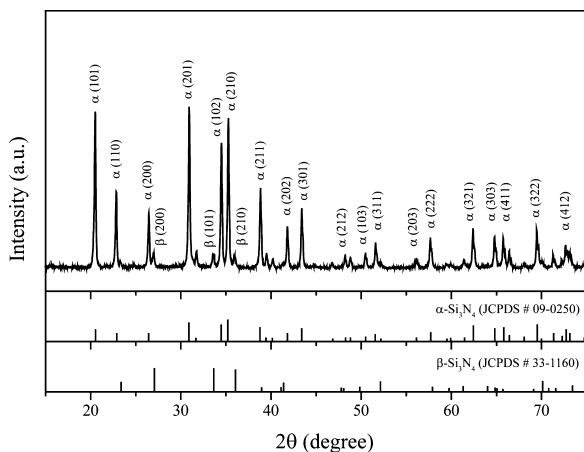

Fig. 2.   X-ray diffraction pattern of the porous silicon nitride ceramic after nitridation of ice-templated silicon structure. Si peaks are not detected, and all of the diffraction peaks related to the α (JCPDS: 09-0250) and β (JCPDS: 33-1160) phases of Si_3N_4 indicate full conversion of Si into Si_3N_4. The relative β/α phase fraction was estimated to be 7.6%.

of hydrogen in the initial stage of the nitriding reaction, which reacts with oxygen from native oxides and prevents it from re-oxidizing the silicon. By lowering the oxygen partial pressure, the hydrogen also renders α-Si_3N_4 the more stable phase.[31,32]

Figure 3 shows SEM images of the porous silicon nitride structure. Figure 3a,b shows the lateral plane of the sample perpendicular to the freezing direction. The lamellar architecture formed with silicon particles was shown to be remained after the nitridation. It is observed that the lamellar walls in the nitrided samples were composed of fibrous whiskers which were revealed as α-Si_3N_4 whiskers in the XRD analysis. Some residues were also observed between the lamellar whisker walls. It is determined that not all the silicon particles volatilized, but some of the silicon particles were remained and converted to silicon nitride particles with direct reaction with nitrogen gas to form α-Si_3N_4, β-Si_3N_4 matte. It was observed that some whiskers were also grown in between the walls. The aligned pore channels and small pores in the whisker walls produced complex porosity, achieving a unique hierarchical porous structure. Figure 3c,d shows the plane parallel to the freezing direction; the pore channels were shown to be straight along the freezing direction. These pore channels could enhance the permeability of the structure, which will be discussed in detail in the later paragraphs describing permeability performance. Figure 3e,f shows the microstructure of porous silicon nitride ceramics from intermediate stage of nitridation. The ice-templated lamellar walls were clearly visible, and whiskers were grown between the walls in the Fig. 3e, and the walls began to deplete by reacting with nitrogen in Fig. 3f.

Based on the observations of the microstructure of porous silicon nitride structure, the formation of a hierarchical structure of pore channels and fibrous whisker lamellar walls can be explained as follows. Figure 4 shows a schematic illustration of the ice-templating and nitridation processes that produced the hierarchical structure of the porous silicon nitride in this study. At first, silicon particles were dispersed in the water with a designated concentration along with additives (Fig. 4a); then, planar ice crystals grew parallel to the freezing direction (Fig. 4b). The particles in the slurry were rejected and expelled by the ice crystals and distributed to form lamellar structures with the ice crystals. Via sublimation of the ice crystals during freeze-drying, only the lamellar walls of silicon particles and a small amount of binders and dispersants remained in the sample green body (Fig. 4c). As the temperature increased, volatilization of the silicon particles in the lamellar walls is began and reacted with nitrogen gas to form fibrous α-Si_3N_4 whis-
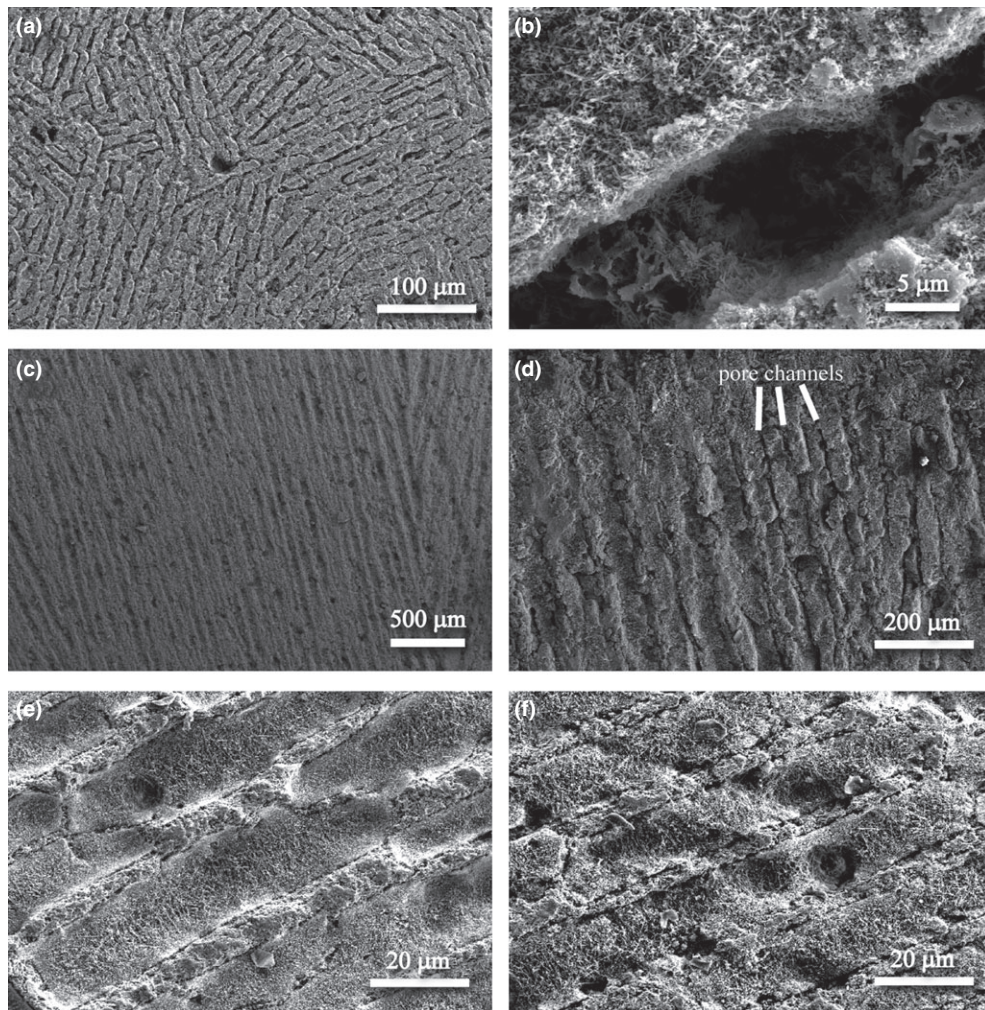
Fig. 3. SEM images of a cross-sectional view of a porous silicon nitride structure after nitridation of the silicon green body prepared by the ice-templating method: (a–b) perpendicular to the freezing direction, (c–d) parallel to the freezing direction, and (e–f) the microstructure of porous silicon nitride ceramics from intermediate stage of the nitridation process.

kers in the pore channels between the lamellar walls of silicon particles (Fig. 4d,e). The volatilization of the silicon particles and the vapor phase reaction with nitrogen in the free surface has been described in elsewhere.[31–34] As the nitridation of the porous silicon structure proceeded, the lamellar walls of silicon particles were partially depleted by volatilization and reaction with nitrogen; fibrous α-Si$_3$N$_4$ whiskers filled in between the original silicon lamellar walls (Fig. 4f). Therefore, the fraction of the ceramic walls and pore channels was reversed to that of the as-templated porous silicon green bodies. In summary, the microstructure consists of (i) silicon nitride α-Si$_3$N$_4$ whisker walls, which are formed by a vapor phase reaction inside the former pore channels of the ice-templated silicon structure, and (ii) pore

channels at the locations of the former Si particle walls with some whiskers and matte forms of α and β-Si$_3$N$_4$, created by direct nitridation of the Si particles.

To investigate the influence of freezing rate on the microstructure of porous silicon nitride ceramics, the four sample structures with freezing rates of 5, 10, 25, and 60 μm/s were observed via optical microscopy, as shown in Fig. 5. The optical microscopy was used for revealing the difference for the microstructures with varying freezing rate in effective way using its low focus of depth. The images show the cross section perpendicular to the freezing direction of the structures that were obtained by different freezing rates, (a) 5 μm/s, (b) 10 μm/s, (c) 25 μm/s, and (d) 60 μm/s with identical slurries of 20 vol. % concentration. Figure 5e–h shows
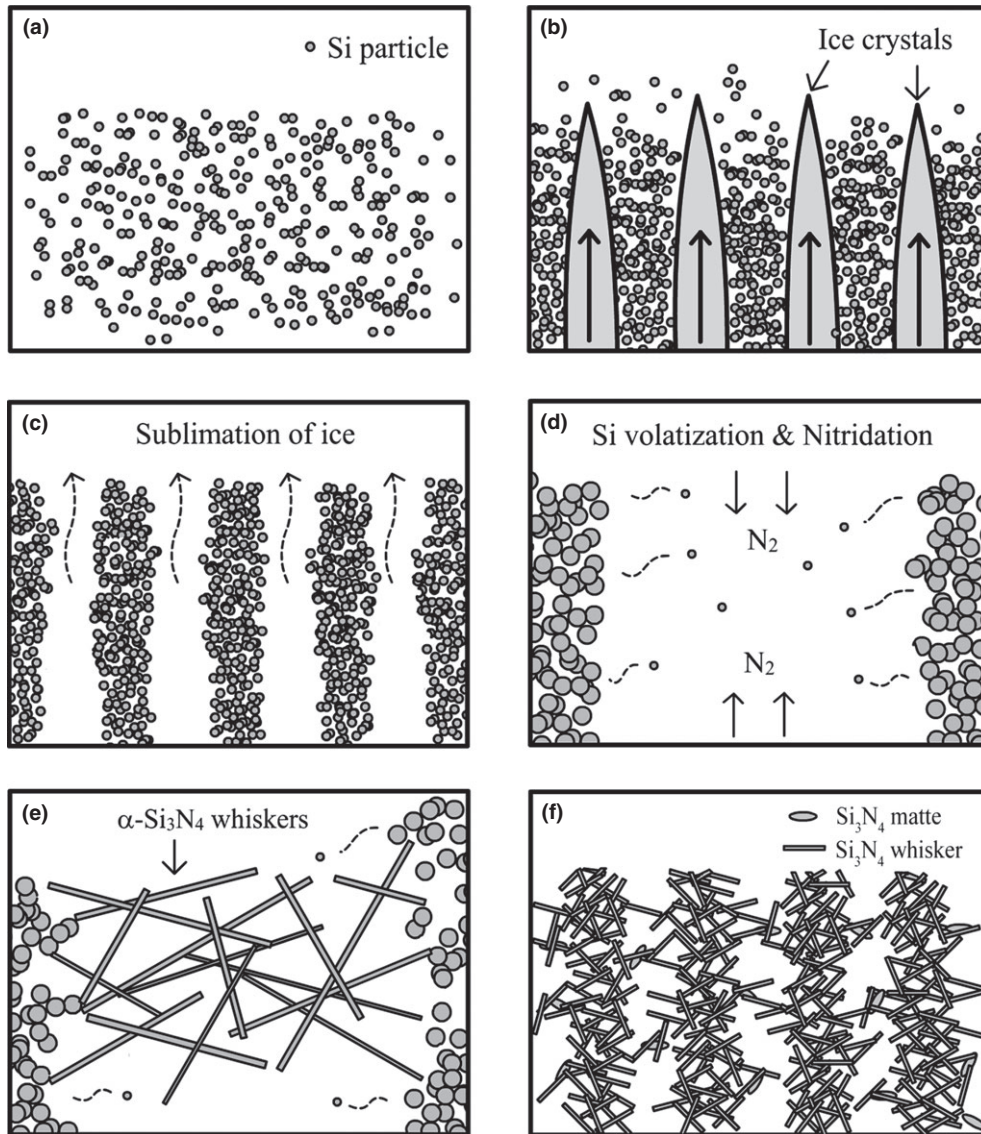
Fig. 4. Schematic illustration of the ice-templating and nitridation processes. (a) Silicon particles dispersed in a slurry, and (b) the silicon particles were redistributed by growing ice crystals, (c) silicon particles formed lamellar porous structure with sublimation of ice, (d) silicon particles volatilized and reacted with nitrogen in nitridation process, (e) silicon particles producing α-Si$_3$N$_4$ whiskers between the lamellar walls by vapor phase reaction. (f) The whiskers were filled closely in lamellar pore channels, and the original lamellar silicon walls were depleted by nitridation to form new pore channels with some residues.

images that are fourfold magnifications of the images shown in Fig. 5a–d, respectively. As mentioned before, the microstructure of the silicon nitride ceramics was lamellar in their architecture in all samples. A significant phenomenon that was observed showed that the wall thickness and spacing of the lamellar structure in the samples decreased distinctly as the freezing rates increased. Deville *et al.*[11] reported that a decrease in the structural wavelength (i.e., the lamellar wall-to-wall distance) in the ice-templating process for alumina slurries

by an increase in the ice-front velocity leads to a decrease in the ice dendrite tip radius due to an increase in supercooling ahead of the ice interface. On the other hand, a decreasing cooling rate leads to an increase in the wavelength of the microstructure.

Figure 6 presents a graph of the lamellar thickness and spacing with varying freezing rates in (a) a linear scale and in (b) a logarithmic scale. The overall measurements show that the dependence of the lamellae structures (i.e., thickness, spacing, wavelength) on the freezing
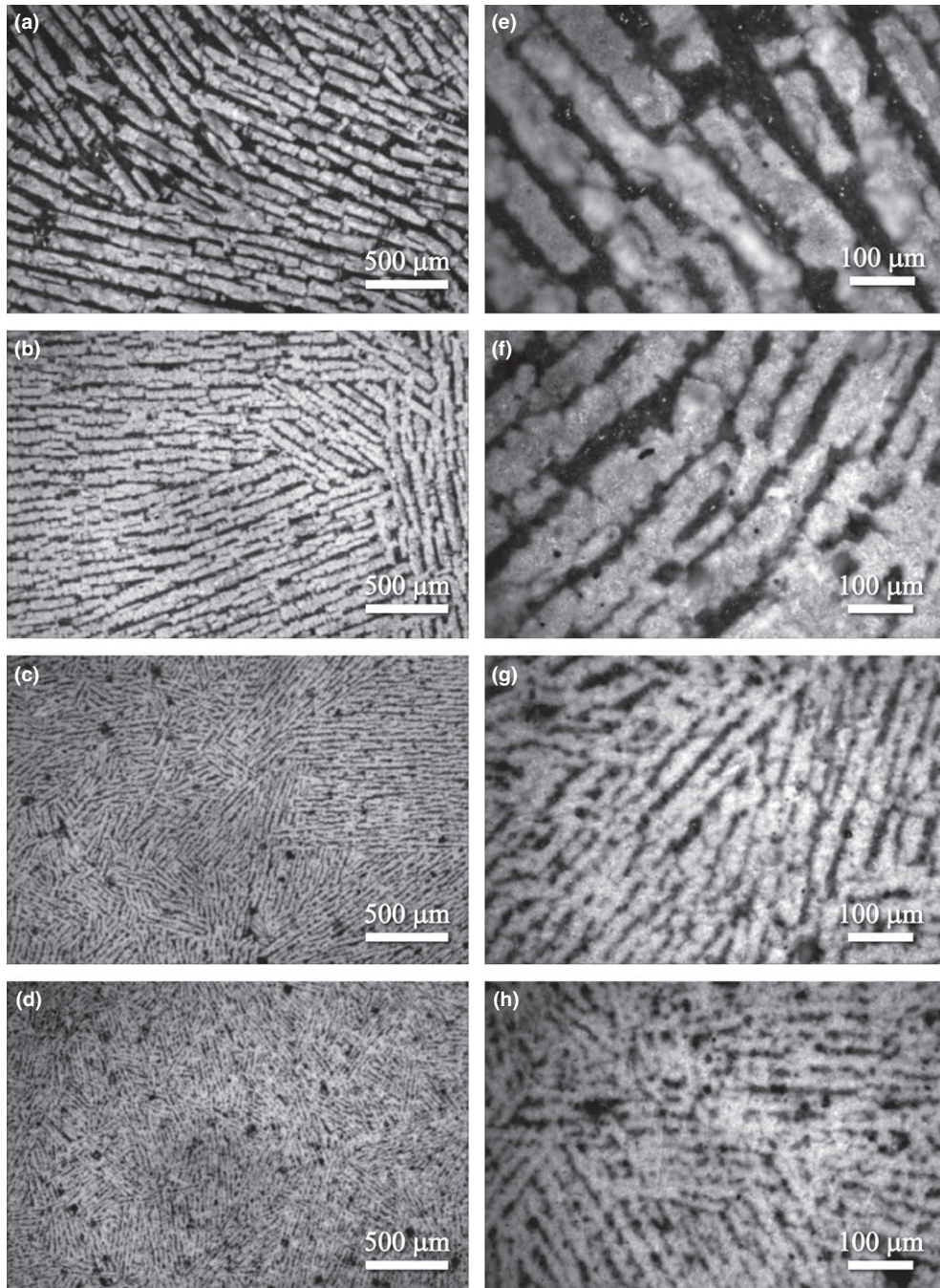
Fig. 5.   Optical microscopy images of lamellar structures created with varying freezing rates of (a) 5 μm/s, (b) 10 μm/s, (c) 25 μm/s, and (d) 60 μm/s. (e–h) Show view of (a–d) magnified fourfold, respectively. The lamellar thickness and the spacing in the samples are shown to decrease with increasing freezing rate.

rate was fitted by an empirically driven common power law $\lambda \propto v^{-n}$.[11] Although the lamellar structure is not an as-templated structure but was nitrided after templating, which reversed the fraction of ceramic walls and pore channels, the approximation is still well described by the

same dependency of the freezing rate on the structures. The fittings through all measured data points yielded power law exponents n from 0.57 to 0.64, which provides guidelines for the dimensional scale of the lamellar structures with varying freezing rates.
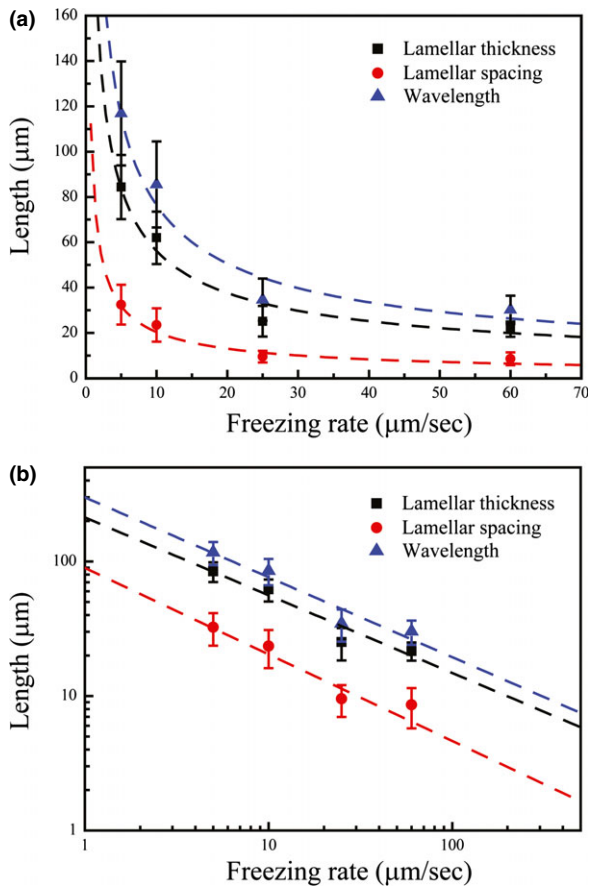
Fig. 6.   Lamellar structures with varying freezing rates in (a) a linear scale and in (b) a logarithmic scale.

Figure 7 shows the pore size distribution of porous silicon nitride ceramics with varying freezing rates. The pore size distribution in the structure showed the same dependency to the lamellar structure with varying freezing rate. The median pore diameter decreased with an increasing freezing rate, which decreased the lamellar size. It could be that the pore diameter is related to the size of the space required for nitridation. The α-Si_3N_4 whiskers formed and grew as nitridation progressed; the whiskers filled finely in the narrow lamellar spaces at a rapid freezing rate; at a slower freezing rate, the whiskers have more freedom to form and grow to fill in the wider lamellar spaces, thus producing more broadly distributed pore sizes that were formed by intersecting whiskers compared to the narrow space presented with more rapid freezing rate. It is also observed that the pore size distribution produced by a slow freezing rate is broader than the distribution produced by a fast freezing rate. There were also secondary peaks around 7 μm, which were determined to be corresponding to pores in aligned pore

channels. The channels were partially filled with the whiskers and matte form of silicon nitrides; therefore, the pore size found to be smaller than the observed lamellar spacing in microscopic images.

Porous ceramics are good candidates for the various engineering applications, and most of these applications require particular mechanical properties of the materials. As porous materials are mostly used in which they are loaded in tension, compressive strength tests generally have been performed to evaluate the property of porous materials. In particular, it is widely known that compressive strength is strongly related to the microstructure of the ceramics; hence, we measured the compressive strength of our ice-templated porous silicon nitride samples with its controlled microstructures affected by varying freezing rate.

The compression test result shown in Fig. 8 reveals correlations between the freezing rate of the samples and their lamellar structures. The compressive strength of the samples increased with an increasing freezing rate, accompanied by a decreased in the lamellar thickness. It is obvious that the higher freezing rate tends to lessen the scale of lamellar structures including lamellar wall thickness and spacing as mentioned in the previous section (Fig. 6).

Compressive strength tests were used to perform for evaluating the strength of porous materials, because the porous materials tend to be used in applications in which they are loaded in compression rather than in tension. To characterize the compressive strength of the porous silicon nitride ceramics we presented, it was needed to consider the materials microstructure, as is widely known, that compressive strength is related to the microstructure, which is a lamellar structure in the study.

The result of the compression tests shown in Fig. 8 reveals correlations between the freezing rate of the samples and their lamellar structures. The compressive strengths of the samples increased with increasing freezing rates. As mentioned before, increasing the freezing rate tends to the decrease the scale of lamellar structures, including lamellar wall thickness and spacing. The compressive strength of the samples was shown to increase with decreasing lamellar thickness (Fig. 8a).

The correlation between the lamellar structure and mechanical properties can be explained in previous studies as follows. At first, it is with regard to the nature of lamellar structure, finer microstructure could enhance the overall structural properties of the material by distributing the stresses on the most concentrated point. Secondly, it may be affected by the pore size. The pore size (i.e., defect size) decreases as the freezing rate increases so that the strength also increases as the defects become
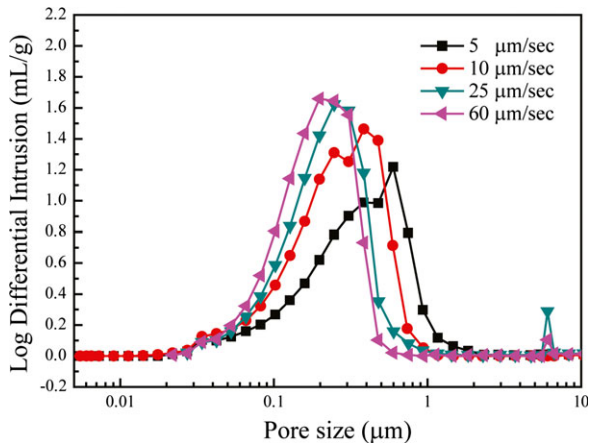
Fig. 7.　Pore size distribution of porous Si₃N₄ ceramics created with varying freezing rates. The size of median pore diameter is shown to decrease with increasing freezing rate due to a decrease in the lamellar structure sizes.

smaller[16]; a similar phenomenon was found in this study with the trend in the pore size distribution. The third explanation is the effect of the bridges between lamellar ceramic walls. Naglieri *et al.*[35] noticed that the bridge density increases exponentially with the freezing front velocity, leading to higher structural strength. To understand the correlation between the microstructure and the compressive strength, it can be explained by applying above mechanisms individually or together in general; however, it is still in lack of interpretation on the lamellar structures to the compressive strength with a direct structural approach.

We proposed a model to interpret the correlation between the compressive strength and the lamellar structure (Fig. 8b). The model is described with a rectangular honeycomb structure composed of lamellar planes of the walls and bridges between the walls. In this rectangular honeycomb model, the cell size and the cell wall thickness decrease as the honeycomb structure becomes finer with increasing number of cells in unit area. In other hands, the ratio of cell wall thickness (t) to the cell size (l) is increased as the structure becomes finer, assuming that the structure remains in same overall density. Figure 8c presents the variation of the compressive strength versus the ratio of cell wall thickness (t) to the cell size (l). The lamellar thickness of the samples was determined as the cell wall thickness to calculate the ratio from the model geometry with the same relative density of the sample structure. According to Gibson and Ashby, the compressive strength of a brittle honeycomb loaded in the out-of-plane direction is dependent on ratio of cell
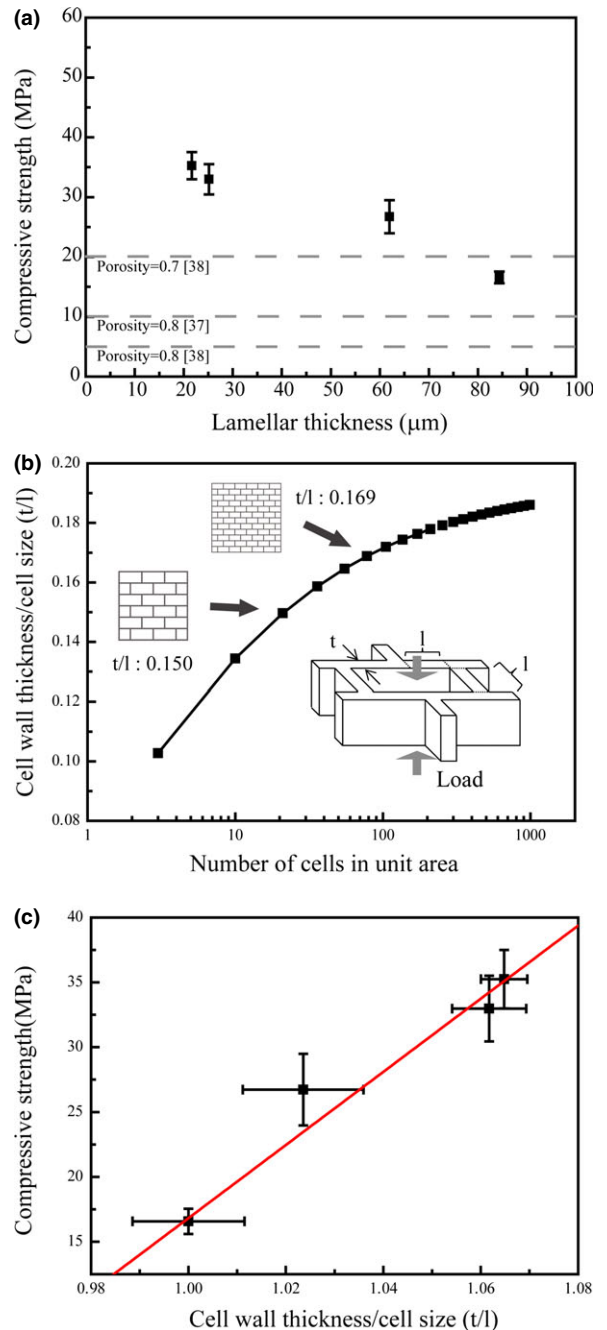

Fig. 8.　(a) Compressive strength of a porous silicon nitride structure along the freezing direction as a function of the slurry freezing rate. (b) The ratio of honeycomb cell wall thickness to the cell size is increasing with decreasing honeycomb scale, that is, increasing numbers of cells (pores) in unit area. (c) The compressive strength was shown to be linearly dependent to the ratio of cell wall thickness to cell size of the structure. This results in higher strength values compared with other porous silicon nitride ceramics with 70–80% porosities.[37,38]

wall thickness to the cell size (t/l).[36] The compressive strength was found to be linearly dependent with the ratio of the cell wall thickness to the cell size, which agrees with the model. Although the microstructure of our material is more complex with lamellar porous ceramic walls composed of α-Si_3N_4 whiskers, this simple model could provide an approach to interpretation of correlation between compressive strength and lamellar structure form ice-templated materials. A detailed investigation of the mechanical properties will be discussed in further studies.

The compressive strength along the freezing direction could be enhanced due to the scaling of aligned hierarchical structure produced by ice-templating and nitridation process, the compressive strength was also found to be higher than those previously reported for porous silicon nitride ceramics with similar porosities.[37,38]

In addition to providing mechanical properties, porous ceramics have many potential applications as filtering materials, including use in high-temperature gas filters. To take advantage of the excellent thermomechanical properties and the filtering capabilities of porous ceramics, a certain level of permeability is required in a filter substrate because pressure drop across the filter diminishes efficiency by increasing back pressure.[29]

Figure 9a shows measurements of the specific flow of air across porous silicon nitride structures frozen at rates of 5, 10, 25, and 60 μm/s. The permeabilities of the samples were calculated to be 0.06, 0.048, 0.041, and 0.035 Darcy ($\sim$$10^{-12}$ m^2), respectively. The permeability of the samples changed by depending on the freezing rate, which has been shown to affect the microstructure of the samples; in this case, the pore size of the samples was primarily related to the permeability.

Many equations have been proposed to estimate the permeability of materials by their structural parameters; these include the Kozeny–Carman equation,[39] Ergun's equation,[40] and Katz–Thompson equation.[41] Permeability is commonly proportional to the square of the pore diameter in these equations, and this relationship is generally expressed in Eq. (3) below, which uses the parameters of pore diameter or grain size (d), a structural factor such as tortuosity (C), and the porosity (φ):

$$\kappa = \frac{d^2}{C}\frac{\varphi^3}{(1-\varphi)^2}. \tag{3}$$

The permeability of the porous silicon nitride ceramics in this study and the previously reported permeabilities of various porous materials[29,42–45] are presented in Fig. 9b along with pore diameters. The lines
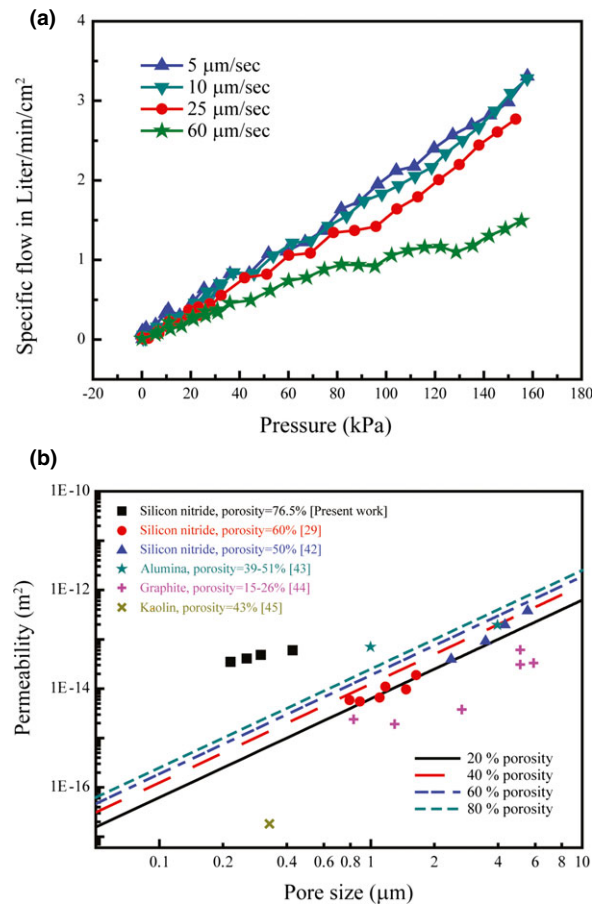

(a)

(b)

Fig. 9. (a) Measurements of flow rates for porous Si_3N_4 structures prepared by the ice-templating method at varying freezing rates; (b) relationship between the Darcy permeability (k) and their pore diameter (d^2) in other studies.[29,42–45] The lines indicate the expected permeability values for the given pore diameters of a porous material with a 20–80% porosity as calculated by Eq. (3).

are drawn from the Eq. (3) with 20–80% of porosity; the permeability data are shown to have a similar tendency with these lines. The permeabilities in this study are shown to be much higher than the expected values with the given pore diameters and porosities. This result is determined to be induced by the structural advantages of the pore channels and the higher porosities achieved by the ice-templating method. Thus, the proposed material will be suitable for the application of filtering particulate matters.

Conclusions

This study focused on the fabrication of porous silicon nitride ceramics using the ice-templating method

with the reaction bonding process. We presented a unique hierarchical porous structure with a high porosity of 76.5% that has complex lamellar pore channels and ceramic walls consisting of fibrous α-Si$_3$N$_4$ whiskers. The evolution of the hierarchical microstructure is discussed and investigated with regard to the influences of freezing rate on the microstructure and properties.

The scale of the pore structure is controlled by changing the freezing rate in the ice-templating method; this is shown to affects both the compressive strength and the gas permeability of the structure. As a result, the porous silicon nitride ceramics fabricated using the proposed method have higher compressive strengths with higher porosities and higher permeability with smaller pore sizes than other conventional porous ceramics. With the enhanced properties of the silicon nitride structure, this material is promising for filtering applications in the future.

Acknowledgments

References

1. K. Ishizaki, S. Komarneni, and M. Nanko, *Porous Materials: Process Technology and Applications*, Kluwer Academic Publishers, Dordrecht, Boston, MA, 1998.
2. S. R. Mukai, H. Nishihara, and H. Tamon, *Catal. Surv. Asia*, 10 [3–4] 116–171 (2006).
3. J. M. Zheng, D. Salamon, L. Lefferts, M. Wessling, and L. Winnubst, *Microporous Mesoporous Mater.*, 134 [1–3] 216–219 (2010).
4. S. Deville, *Adv. Eng. Mater.*, 10 [3] 155–169 (2008).
5. L. Y. Hu, Y. M. Zhang, S. L. Dong, S. M. Zhang, and B. X. Li, *Ceram. Int.*, 39 [6] 6287–6291 (2013).
6. A. Lasalle, C. Guizard, E. Maire, J. Adrien, and S. Deville, *Acta Mater.*, 60 [11] 4594–4603 (2012).
7. S. W. Yook, *et al.*, *Acta Biomater.*, 8 [6] 2401–2410 (2012).
8. M. M. Porter, *et al.*, *Mater. Sci. Eng. A Struct. Mater.*, 556 741–750 (2012).
9. T. Fukasawa, Z. Y. Deng, M. Ando, T. Ohji, and Y. Goto, *J. Mater. Sci.*, 36 [10] 2523–2527 (2001).
10. U. G. K. Wegst, M. Schecter, A. E. Donius, and P. M. Hunger, *Philos. Trans. A Math. Phys. Eng. Sci.*, 368 [1917] 2099–2121 (2010).
11. S. Deville, E. Saiz, and A. P. Tomsia, *Acta Mater.*, 55 [6] 1965–1974 (2007).
12. M. Pradhan and P. Bhargava, *J. Am. Ceram. Soc.*, 88 [4] 833–838 (2005).
13. E. Munch, E. Saiz, A. P. Tomsia, and S. Deville, *J. Am. Ceram. Soc.*, 92 [7] 1534–1539 (2009).
14. K. Araki and J. W. Halloran, *J. Am. Ceram. Soc.*, 88 [5] 1108–1114 (2005).
15. R. F. Chen, C. A. Wang, Y. Huang, L. G. Ma, and W. Y. Lin, *J. Am. Ceram. Soc.*, 90 [11] 3478–3484 (2007).
16. S. Deville, E. Saiz, and A. P. Tomsia, *Biomaterials*, 27 [32] 5480–5489 (2006).
17. K. K. Mallick, J. Winnett, W. van Grunsven, J. Lapworth, and G. C. Reilly, *J. Biomed. Mater. Res., Part A*, 100A [11] 2948–2959 (2012).
18. Y. Chen, J. Bunch, T. S. Li, Z. P. Mao, and F. L. Chen, *J. Power Sources*, 213 [9] 3–9 (2012).
19. P. Gannon, S. Sofie, M. Deibert, R. Smith, and V. Gorokhovsky, *J. Appl. Electrochem.*, 39 [4] 497–502 (2009).
20. E. P. Gorzkowski and M. J. Pan, *JOM*, 66 [2] 261–269 (2014).
21. S. Roy and A. Wanner, *Compos. Sci. Technol.*, 68 [5] 1136–1143 (2008).
22. M. E. Launey, *et al.*, *Acta Mater.*, 57 [10] 2919–2932 (2009).
23. M. H. Bocanegra-Bernal and B. Matovic, *Mater. Sci. Eng. A Struct. Mater.*, 500 [1–2] 130–149 (2009).
24. K. Hirao, K. Watari, H. Hayashi, and M. Kitayama, *MRS Bull.*, 26 [6] 451–455 (2001).
25. J. F. Yang, G. J. Zhang, and T. Ohji, *J. Am. Ceram. Soc.*, 84 [7] 1639–1641 (2001).
26. C. Kawai and A. Yamakawa, *J. Mater. Sci. Lett.*, 17 [10] 873–875 (1998).
27. T. Waschkies, R. Oberacker, and M. J. Hoffmann, *Acta Mater.*, 59 [13] 5135–5145 (2011).
28. K. Nakagawa, N. Thongprachan, T. Charinpanitkul, and W. Tanthapanichakoon, *Chem. Eng. Sci.*, 65 [4] 1438–1451 (2010).
29. Y. J. Park, H. D. Kim, and J. W. Halloran, *Int. J. Appl. Ceram. Technol.*, 8 [4] 809–814 (2011).
30. C. P. Gazzara and D. R. Messier, *Am. Ceram. Soc. Bull.*, 56 [9] 777–780 (1977).
31. M. Barsoum, P. Kangutkar, and M. J. Koczak, *J. Am. Ceram. Soc.*, 74 [6] 1248–1253 (1991).
32. A. J. Moulson, *J. Mater. Sci.*, 14 [5] 1017–1051 (1979).
33. H. M. Jennings, *J. Mater. Sci.*, 18 [4] 951–967 (1983).
34. R. G. Pigeon, A. Varma, and A. E. Miller, *J. Mater. Sci.*, 28 [7] 1919–1936 (1993).
35. V. Naglieri, H. A. Bale, B. Gludovatz, A. P. Tomsia, and R. O. Ritchie, *Acta Mater.*, 61 [18] 6948–6957 (2013).
36. L. J. Gibson and M. F. Ashby, *Cellular Solids: Structure and Properties*, Cambridge University Press, Cambridge, NY, 1999.
37. L. Y. Yin, *et al.*, *Key Eng. Mater.*, 519 [28] 1–6 (2012).
38. Z. X. Lu, Q. Liu, H. T. Han, and D. H. Zhang, *Mater. Sci. Eng. A Struct. Mater.*, 559 201–209 (2013).
39. P. C. Carman, *Trans. Inst. Chem. Engrs.*, 15 150 (1937).
40. S. Ergun, *Chem. Eng. Prog.*, 48 89–94 (1952).
41. A. J. Katz and A. H. Thompson, *Phys. Rev. B*, 34 [11] 8179–8181 (1986).
42. G. Topates, L. Mammitzsch, U. Petasch, J. Adler, F. Kara, and H. Mandal, *J. Eur. Ceram. Soc.*, 33 [9] 1545–1551 (2013).
43. T. Isobe, Y. Kameshima, A. Nakajima, K. Okada, and Y. Hotta, *J. Eur. Ceram. Soc.*, 27 [1] 53–59 (2007).
44. W. A. Anderson, *Carbon*, 4 [1] 107–114 (1966).
45. J. H. Eom, Y. W. Kim, and I. H. Song, *J. Korean Ceram. Soc.*, 50 [5] 341–347 (2013).